Targeted imaging in oncologic surgery : preclinical studies utilizing near-infrared fluorescence and radioactivity

Boonstra, M.C.

Chapter 7

Preclinical evaluation of a novel EpCAM-targeting fluorescent imaging agent to improve intra-operative cancer visualization

Supplementary data on ePUB

ABSTRACT

Introduction: Tumour-specific fluorescent-labelled imaging agents are moving towards the clinic, supporting surgeons with real-time intraoperative feedback about tumour location and incomplete resections. Due to its general and high overexpression on carcinomas, EpCAM (Epithelial Cell Adhesion Molecule) is considered as one of the most promising pluripotent tumour targets. This study investigates F(ab)/800CW, a novel antibody-fragment based NIR fluorescent agent.

Methods: F(ab) production, conjugation and binding capacities were investigated and validated using, HPLC, spectrophotometry and cell-based assays. *In vivo* dose escalation-, blocking- and biodistribution studies (using both fluorescence and radioactivity) were performed, next to imaging of clinical relevant orthotopic xenografts for breast and (colo)rectal cancer.

Results: F(ab)/800CW binds EpCAM with high specificity *in vitro*, which was validated using *in vivo* blocking experiments. The optimal dose was between 1-5 nmol in mice, which corresponds with 0.16-0.8mg/kg human equivalent dose. Biodistribution showed high accumulation of F(ab)/800CW in tumours and metabolizing organs. Breast and (colo)rectal tumours could clearly be visualized from 8h post-injection up-to 96h with high TBRs (>2), while the agent already showed full tumour penetration between 1 and 4 hours.

Conclusion: This study describes the preclinical work-up and feasibility of a novel EpCAM-recognizing agent to visualize (colo)rectal and breast tumours during image-guided resections, with the potential to be translated for clinical use.

Surgical relevance

The epithelial cell adhesion molecule (EpCAM) is abundantly overexpressed on carcinomas and is recognized as one of the most promising, pluripotent targets for tumour imaging. The innovative EpCAM-directed NIR-fluorescent imaging agent, presented in our study, is expected to provide the surgeon with a robust, sensitive and selective diagnostic tool. It aids in detecting (residual) cancer, positive lymph nodes, local metastasis and incomplete resections in real-time during (laparoscopic) surgery. Wide implementation of tumour-specific (NIR) fluorescence imaging has the potential to bring surgery to the next level; improving clinical practice and enabling personalized precision surgery by visualizing structures and lesions, making surgery safer and more precise.

INTRODUCTION

Prognosis after cancer surgery mainly depends on the completeness of the surgical resection. Intraoperative detection of tumour margins, nodules and positive lymph nodes can be challenging due to intricate anatomy or neo-adjuvant (chemo) radiation, which induces scar tissue and alters morphology, hampering clear tumour identification. A relatively novel technique aiding inthe intraoperative identification of these tumours is Fluorescent-Guided Surgery (FGS). FGS is based on (near-infrared, NIR) fluorescent dyes in combination with a dedicated imaging system and is already widely investigated for sentinel lymph node mapping, anastomosis perfusion and bile duct imaging [1]. Conjugating fluorescent dyes to specific tumour-recognizing ligands, like an antibody or a peptide, dramatically enhances the specificity of this technique, and various tumour specific agents have already shown feasibility in early clinical trials [1, 2].

Not all tumour-associated biomarkers are suitable as target; prerequisite is expression on the cellular membrane with at least 10-times higher densities compared to surrounding normal cells [3]. The Epithelial Cell Adhesion Molecule (EpCAM) was among the first human tumour-associated antigens discovered and was identified by a number of independently developed monoclonal antibodies (mAb) 17-1A, 323/A3, and MOC31 [4]. EpCAM is a 40kD type I transmembrane glycoprotein involved in cell-to-cell interactions and adhesions [5]. Under physiological conditions, EpCAM is present at low numbers on the basolateral surface of epithelial cells and in undifferentiated pluripotent stem cells [6]. But, it is overexpressed in virtually all epithelial cancers and expression is conserved with cancer progression and metastasis [7]. Recently, EpCAM was associated with cellular signalling processes and demonstrated to play a prominent role in tumour cell migration, proliferation and differentiation [8]. Extreme overexpression (100-1000 fold) of EpCAM has been found in colorectal, gastric, oesophageal, head-and-neck, breast

and gynaecological cancers with cell surface copy numbers ranging between 100.000 and 300.000 [9-11]. Consequently, EpCAM targeting antibodies were studied in clinical phase I, II and III trials in various cancer types such as ovarian-, gastric- and head-and-neck cancer and peritonitis carcinomatosis [12-14].

In this study, we combined two well-known clinically tested components: a MOC31 antibody derived F(ab) fragment [15] and the fluorophore IRDye800CW [16, 17]. The antibody fragment has already been tested in preclinical and clinical settings as the (therapeutical) immunotoxin VB6-845, constructed as a recombinant fusion protein [18]. Clinical relevance of fluorophore IRDye800CW was already shown in an early phase clinical trial conjugated to cetuximab. [19]. The overall aim of this study was to develop, produce and validate a novel EpCAM-specific NIR fluorescent imaging agent, called F(ab)/800CW. Application of F(ab)/800CW during oncological surgery will aid in real-time detection of a wide variety of epithelial cancers, assist clinical decision making and improve treatment strategies for cancer patients, including (colo)rectal and breast cancer, in the near future.

MATERIALS AND METHODS

Human samples and staining

Tissue blocks from 10 patients who underwent resection of rectal cancer between 2014 and 2015 were obtained at the Pathology Department of the Leiden University Medical Centre (LUMC). Of these 10 patients, 5 patients received, and 5 patients did not receive neo-adjuvant therapy. Paraffin-embedded tumour blocks of rectal cancer tissue as well as adjacent normal rectal tissue were obtained. After sectioning, these slides were stained for EpCAM using commercially available MOC31 (Millipore, MA, USA) in a concentration of 1:10.000. After overnight incubation of the sections with MOC31, DAKO envision + HRP anti-mouse was added for 30 min (K4001; DAKO Cytomation, Glostrup, Denmark) followed by diaminobenzidine solution (DAB+; DAKO Kit) to visualize EpCAM expression. All sections were counterstained with hematoxylin, dehydrated and finally mounted with pertex. All samples were handled in an anonymous fashion according to the national ethical guidelines ('Code for Proper Secondary Use of Human Tissue', Dutch Federation of Medical Scientific Societies) and were approved by the Institutional Ethics Committee of the Leiden University Medical Center (LUMC).

F(ab) production, conjugation and stability

VB5-845d is a T-cell epitope depleted F(ab) version of the anti-EpCAM F(ab) deBouganin fusion protein, VB6-845. To express VB5-845d in E. coli supernatant, a dicistronic unit was created where the heavy and light chains were preceded by a PelB leader sequence. The

insert was placed under the control of the arabinose promoter and cloned into a pING plasmid. The resulting VB5-845d/pING plasmid was then transformed into E 104 E. coli host. After L-arabinose induction, the presence of soluble VB5-845d F(ab) protein in the supernatant was detected by Western blot using a human anti-Kappa antibody coupled to HRP (Sigma, St Louis, MO). In a 20 L Bioreactor containing 15 L of glycerol minimum media, transformed E. coli E104 cells were grown to an OD600 of 50 and induced with L-arabinose. Following induction, the supernatant was collected by centrifugation, clarified by microfiltration, concentrated and diafiltrated prior to loading onto a KappaSelect column (GE Healthcare Life Sciences, Mississauga, ON). After the column was washed with equilibration buffer, bound VB5-845d was eluted with 0.1 M Glycine-HCl, pH 2.5 and neutralized to pH 7.0 with Tris buffer. The fractions containing VB5-845d were then flowed-through a Q-sepharose column (GE Healthcare Life Sciences, Mississauga, ON) and the effluent loaded on to an SP-sepharose (GE Healthcare Life Sciences, Mississauga, ON). Bound VB5-845d was eluted, filter sterilized and frozen at -20°C. Purity was confirmed by Coomassie staining and SE-HPLC and identity by Western blot analysis. Protein concentration was determined by BCA (Thermo Fisher Scientific, Waltham, MA).

IRDye800CW NHS-ester (λex= 773 nm, λem= 792 nm) was bought from Licor (LI-COR, Lincoln, NE, USA) and DOTA was bought from Sigma, both stored according to manufacturer protocol.

The EpCAM-specific F(ab) fragment was covalently conjugated to IRDye800CW and DOTA using N-Hydroxysuccinimide (NHS) ester chemistry against primary amines following manufacturer protocol (Thermo Scientific, USA) and is briefly described in the supplementary data. For IRDye800CW Maldi-TOF analyses were performed to evaluate labelling ratios. Stability of the fluorescent conjugate was evaluated in various test conditions, including storage at RT/37°C for 24 hours, lyophilisation, different pH values, shake/shear stress and multiple freeze/thaw cycles. Likewise, integrity over time in serum and plasma was evaluated using gel-electrophorese.

Human cancer cell lines

A total of four human cancer cell lines were used; two from colorectal cancer origin (HT-29 and Colo320) and two from breast cancer origin (MCF-7 and MDAco). All cell lines were free of Mycoplasma species and were cultured in RPMI1640 (PAA) supplemented with 10% fetal bovine serum (Gibco) and 100 I.U./mL penicillin/ streptomycin (PAA) in a humidified incubator at 37°C and 5% CO2. The HT-29-luc2 cell-line was established and validated by our own research group [20].

Flow-cytometry and fluorescent affinity assays

Identical protocols were used as previously described [20] and are detailed in the Supplementary Materials.

Animal models

The Animal Welfare Committee of the LUMC approved all animal experiments for animal health, ethics, and research. All animals received humane care and maintenance in compliance with the 'Code of Practice Use of Laboratory Animals in Cancer Research" (Inspectie WandV, July 1999). Same animal models were used as previously described [21] and are extensively described in the supplementary materials. In short, six week-old athymic female mice were either injected subcutaneously with HT-29-luc2 cells (500.000 cells per spot) at 4-sides on the back, to induce subcutaneously (colo)rectal tumours, or were inoculated with 250.000 MCF-7-luc2-cGF cells in two contralateral mammary fat pads, to induce orthotopic breast tumours. For the (colo)rectal orthotopic model, subcutaneously growing HT-29-luc2 tumours were harvested, cut in small fragments, and transplanted onto the cecal wall.

NIR-fluorescent cameras

Imaging was performed using the PEARL small animal imager (LI-COR, NE, USA) [21] and the Artemis imaging system (Quest Medical Imaging, the Netherlands). Identical imaging set-ups were used as recently described [22]. Detailed information is given in the supplementary material section.

In vivo specificity

The *in vivo* binding specificity of F(ab)/800CW was explored using a blocking experiment. Mice bearing subcutaneous (colo)rectal tumours (HT-29-luc-2) received 4 hours prior to IV injection of F(ab)/800CW (50 µg, 1 nmol) an intra-peritoneal injection of a 10 times higher dose of unlabeled F(ab) (500 µg, 10 nmol) (N=4). NIR fluorescent images were acquired at 24 and 72 hours post-injection with both the PEARL and the Artemis imaging system. After the last measurement, animals were sacrificed and signal-to-background ratios (SBR) were calculated, by drawing regions of interest (ROIs) on tumours and surrounding tissue on the fluorescence images.

In vivo binding characteristics, dose finding and biodistribution

When the subcutaneous HT-29 colorectal tumours were 36±6mm^2, either 1/16 nmol (3.25 µg), 1/4 nmol (13 µg), 1 nmol (52 µg), 5 nmol (260 µg), 10nmol (520 µg) or 20nmol (1040 µg) F(ab)/800CW was intravenously injected (N=3 per dose group). At 4, 8, 24, 48, 72 and 96 hours after injection, fluorescence was measured using the Pearl® and the Artemis imaging system. Biodistribution studies, using fluorescence, were performed in mice bearing HT-29 tumours with either MOC31/800CW or F(ab)/800CW or control mice without injection of F(ab)/800CW. In total, 6 mice were injected with 1 nmol of MOC31/800CW (150µg) and sacrificed at 24 (n=3) or 72 hours (n=3) post injection. The

same experiment was performed in mice injected with F(ab)/800CW (52µg) (n=6) and control mice (N=6).

Radiolabelling and biodistribution

Radiolabelling was performed by dissolving F(ab)/DOTA in 0.1M HEPES buffer (10µg/100µL) and adding indium (III)chloride (35MBq InCl3, Covidien-Mallinckrodt, Dublin, Ireland). After 30 min of incubation on the shaker, labelling was validated by HPLC (JASCO, USA). In all cases, labelling efficacy was >90%.

To study the bio-distribution, 6 mice were intravenously injected with 50µg (1 nmol) of F(ab)/DOTA/111In. Mice were respectively 24 (N=3) and 72 hours (N=3) after injection sacrificed and organs were excised, weighted, and counted for radioactivity with a gamma counter (Wizard2 2470 automatic gamma scintillation counter, Perkin Elmer, USA). The %ID/weight was calculated by dividing the MBq measured in tissue/injected dose *100% by weight of tissue.

Tumour penetration

Tumour penetration of F(ab)/800CW was assessed in (colo)rectal tumours, obtained from 8 mice bearing subcutaneous HT-29 tumours. Mice were sacrificed respectively 1 (n=2), 4 (n=2), 8 (n=2) and 24 hours (n=2) after injection of either 1 or 10nmol F(ab)800CW. Tumours were snap-frozen in isopentane and kept at -80 degrees Celsius. Tissues were sectioned at 10µm, stained with DAPI after which fluorescence imaging was performed using a Leica DM5500B digital microscope (Leica Microsystems B.V., Son, the Netherlands).

Statistical analyses

Statistical analysis and generation of graphs was performed using GraphPad Prism software (version 5.01, GraphPad Software Inc, La Jolla, California, USA). Differences between groups in the *in vitro* binding assays were analysed using the Mann-Whitney U test. Tumour-to-background ratios were calculated by drawing regions of interest (ROIs) on fluorescence images from the Pearl® small animal imager or Artemis imaging system to extract mean signal from tumours and organs. Ratios were calculated by dividing each value by the mean fluorescence signal detected in the surrounding tissue and/or in the blood and reported as mean and standard deviation. The two-way repeated measurement ANOVA, used to assess the relation between TBRs in different dose groups and time points, was corrected using the Bonferroni correction. P-values equal or lower than 0.05 were considered significant.

RESULTS

EpCAM expression on human rectal (cancer) tissues

Normal rectal tissue did show some positivity for EpCAM. Expression was mostly limited to the mucosa, in shedding senescent colonocytes, located at the tip of the villi (Figure 1A). All rectal cancer tissues showed heterogeneous EpCAM expression, with a circumferential staining pattern (Figure 1B and 1D). There was no difference in EpCAM expression on tumour cells and in normal rectal tissue between patients who did not (Figure 1B & 1C) or did (Figure 1D & 1E) receive neo-adjuvant therapy.

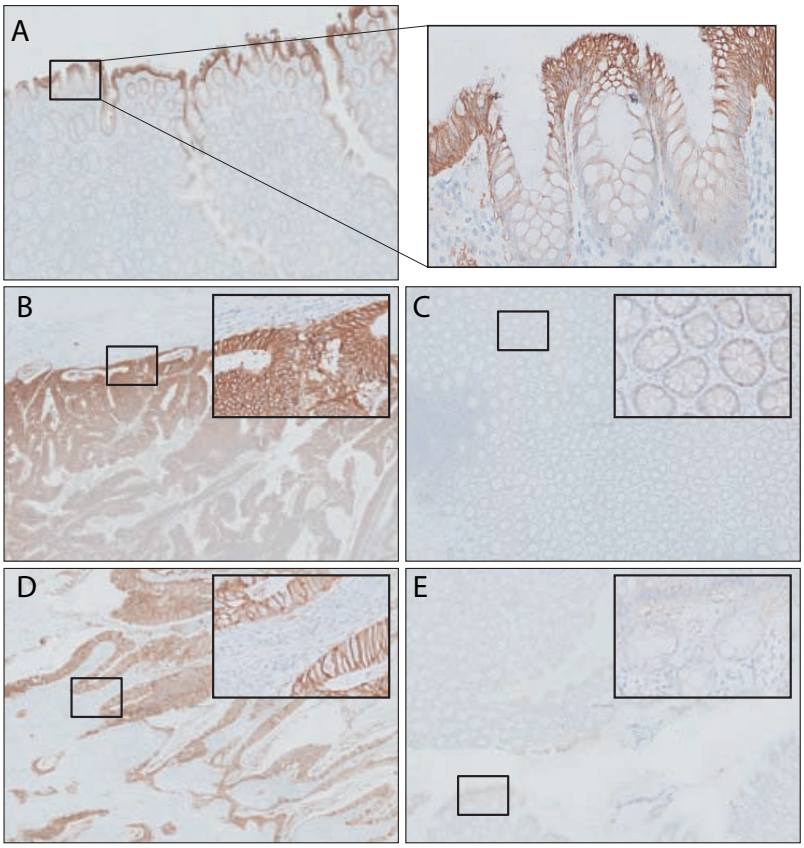

Figure 1 A) Example of EpCAM expression on normal rectal tissue; EpCAM expression is confined to the luminal side of the epithelium. B) Example of EpCAM expression on a distal rectal tumor of a patient who did not receive neoadjuvant therapy. C) EpCAM expression on the corresponding normal rectal tissue of the same patient. D) EpCAM expression of a proximal rectal cancer of a patient who has been treated with neoadjuvant therapy. E) EpCAM expression on the corresponding normal rectal tissue of the same patient. (5x and 40x enlargement)

F(ab) conjugation, stability and binding capacity

High expression of EpCAM was measured on HT-29 and MCF-7 cell lines while almost no expression was seen on the control cell lines Colo-320 and MDAco (Figure 2A). Before

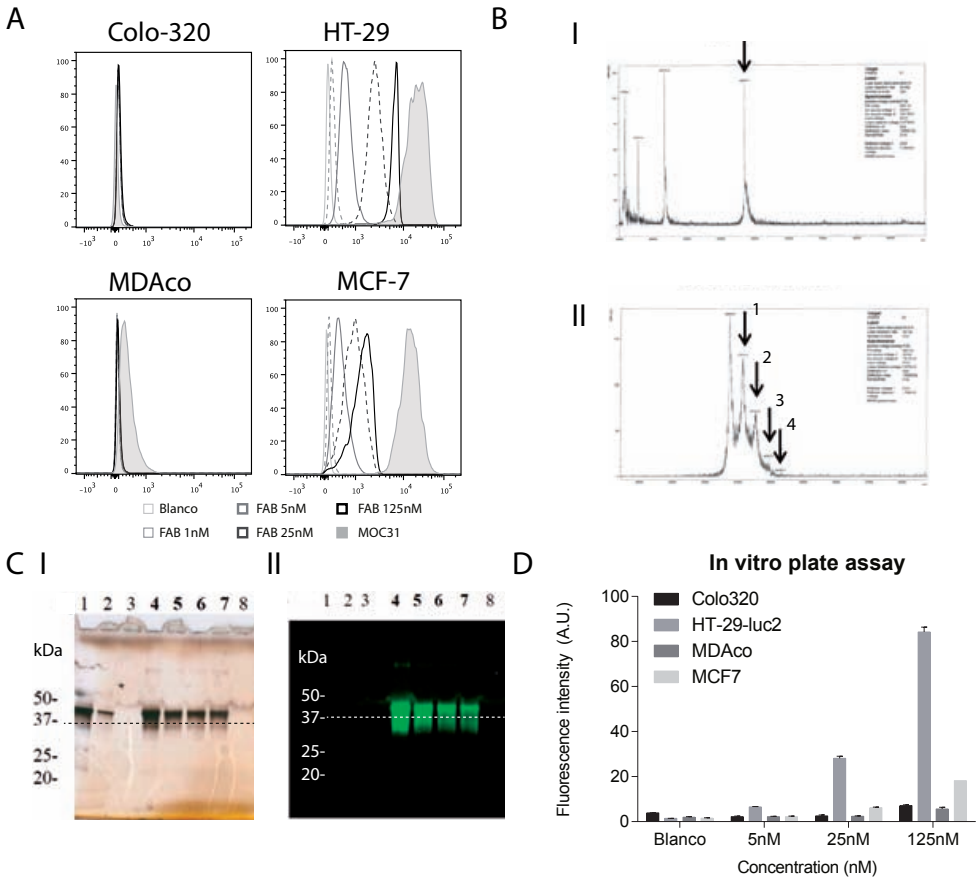

Figure 2 A) Binding capacity of F(ab) for EpCAM using flow-cytometry. MOC31 confirmed the high and low expression levels of EpCAM on the tumor cells. Enhancing the concentration of F(ab) resulted in an increase in signal on the cells with high EpCAM expression. B) I, Maldi-TOF analysis of F(ab) showed one clear peak at 46870 Da with a purity of >98%. II, extra peaks appeared at 47816Da (1), 48795Da (2), 49820Da (3) and 50761Da (4) representing respectively 1, 2, 3 and 4 IRDye800CW labels per F(ab). C) Stability was evaluated using SDS-PAGE gel (4-20%). Unconjugated F(ab) in lane 1 (10µg) and lane 2 (1µg) and F(ab)/800CW in lane 4 (10 µg), lane 5 (5 µg), lane 6 (5 µg) and lane 7 (5 µg) while lane 3 and lane 8 are empty. F(ab)/800CW was clearly visible at approximately 45kDa both with silver staining and fluorescence. D) Plate assay analysis showed retained binding capacity of F(ab)/800CW on all four cell lines after conjugation. Increasing the concentration increased the fluorescent intensity for the high expressing cell lines.

conjugation F(ab) showed to be >98% pure (Figure 2B I). After conjugation, Maldi-TOF analysis indicated that the majority of F(ab) molecules were conjugated with 1-4 dye molecules (Figure 2B II). The stability of F(ab)/800CW (45 kDa) was shown using SDS-PAGE (Figure 2C I) and by NIR fluorescent imaging (Figure 2C II) and no degradation products were seen. Optimal fluorescence signal was obtained with labelling ratios around 1.5 (data not shown). Binding experiment showed that higher concentrations of F(ab)/800CW resulted in higher signals on the EpCAM expressing cell lines, while almost no signals were measured in the low expressing control cell lines (Figure 2D).

In vivo biodistribution

At 24 hours, mean fluorescence intensity (Arbitrary Units, A.U.) of blood was 0.041 ± 0.008 and 0.015 ± 0.005 for respectively MOC31/800CW and F(ab)/800CW, while this was 0.006 ± 0.002 and 0.001 ± 0.000 at the 72h time-point (Figure 3A & B). MOC31/800CW showed relatively high background values, resulting in similar or increasing signals in all measured organs (Figure S1) between the 24h and 72h time-points compared to F(ab)/800CW. The highest values were seen in metabolizing organs and in tumours at 72h (Figure 3A). Control animals showed relatively high ratios due to the absence of exogenous administered fluorophores (Figure 3A and Table S3). Biodistribution of F(ab)/800CW showed a significant increase of fluorescence signals over time (Figure S2) and significant higher signals in liver, kidneys, tumour and bladder compared to control mice (Figure 3B). A blood half-life time of 2-4 hours could be measured. Tumour-to-background ratios (TBR) were significantly higher for F(ab)/800CW compared to its full size variant MOC31/800CW at both 24h and 72h post-injection (Figure 3C).

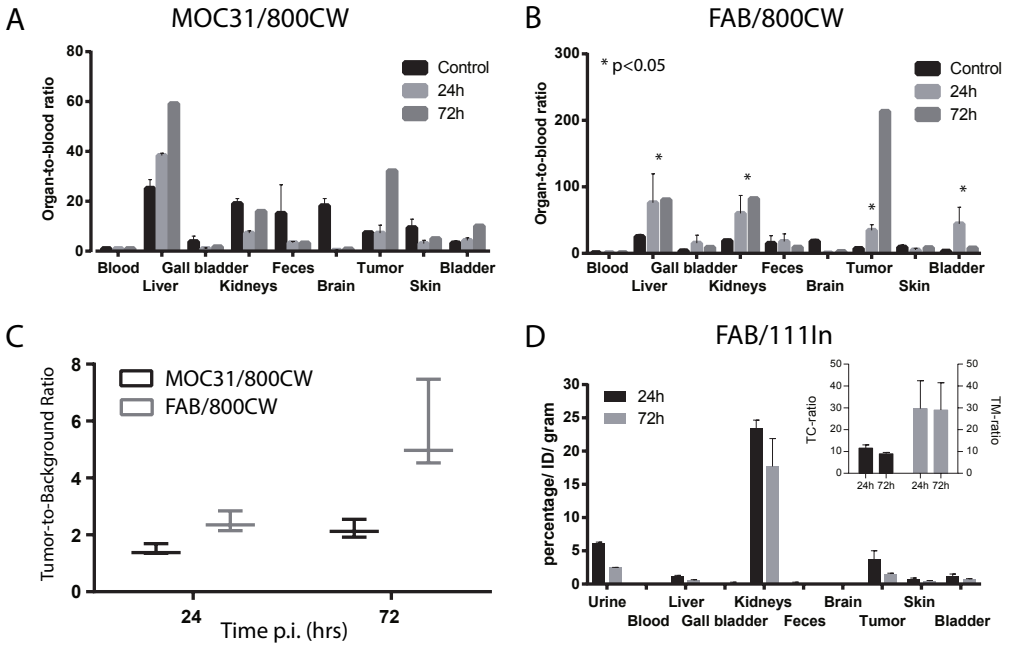

Figure 3 A) Biodistribution of MOC31/800CW presented as organ-to-blood ratio at 24 and 72h post injection. High fluorescence was seen in the feces, mainly due to fluorescent food. B) Biodistribution of F(ab)/800CW presented as organ-to-blood ratio at 24 and 72h. Significant high signals were measured between control mice and liver, kidneys, tumour and bladder. C) Significant higher TBRs were measured for F(ab)/800CW both at 24 and 72h post injection compared to MOC31/800CW. D) Biodistribution of F(ab)/111In showed as %/ID/gram at 24 and 72h post-injection. Tumour-to-colon (TC) ratios were 11.52 ± 1.509 and 8.91 ± 0.686 at respectively 24 and 72h while the tumour-to-muscle (TM) ratio was higher: 29.64 ± 12.753 and 29.01 ± 12.503 for the same time points.

Quantitative measurements of the biodistribution were performed using F(ab)/111Indium (1nmol). Mean activities for the mice sacrificed at 24h post injection were 5.67 ± 0.142 and at 72h, 5.15 ± 0.329 (MBq, mean±SD). The biodistribution study confirmed accumulation of F(ab)/111In in subcutaneous colorectal tumours and excreting organs such as the liver and the kidneys at 24h, with significant lower values at the 72h time-point (selection in Figure 3D and full in Figure S4). Compared to the signals from the intestine, relatively high signals were observed in the skin, thereby influencing TBRs, as also seen with NIR fluorescence in this subcutaneous model. Mean tumour-to-colon (TC) ratio was 11.5 ± 1.5 at 24h and 8.9 ± 0.7 at 72h and mean tumour-to-muscle (TM) ratio was 29.6 ± 12.8 at 24h and 29.0 ± 12.5 at 72h.

In vivo blocking study and dose optimization

EpCAM specificity of F(ab)/800CW was further validated using a blocking experiment. 24h post-injection, the group with a pre-injection of unlabelled F(ab) showed significant lower TBRs compared to the group without the pre-injection (2.1±0.4 vs. 6.8±1.7,p<0.05) and the difference increased further at 72h (3.0±0.6 vs. 10.0±3.5, p<0.05) (Figure 4A).

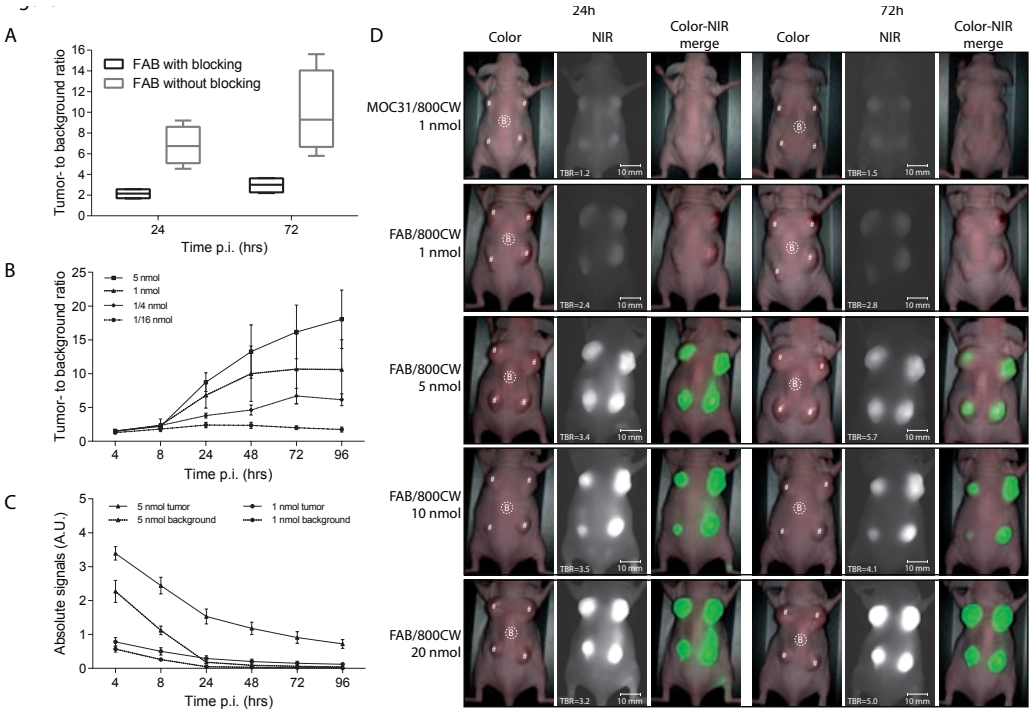

Figure 4 A) Blocking with unlabelled F(ab) fragments significantly (p<0.05) decreased the tumour-to-background ratios at both the 24h (6.81 ± 1.651 vs. 2.34 ± 0.421) and 72h (10.01 ± 3.544 vs. 2.96 ± 0.638) time-point. B) Tumour-to-background ratios (TBR) are shown over time for the 1/16 to 5 nmol dose groups. C) Absolute tumour and background signals are shown for the 5nmol and 1nmol dose groups. D) Examples of *in vivo* images of mice bearing subcutaneous tumours acquired at 24 and 72h post injection with MOC31/800CW or different doses of F(ab)/800CW. The white regions of interest are used as background to calculate TBRs. All images are normalized and acquired with the Artemis imaging system. (# tumours of different sizes)

Dose optimization studies showed increasing TBRs for all doses at the first measurement time points (Figure 4B & S5). For the 24h time-point, a significant difference was observed between 1nmol versus 1/16nmol ($p<0.05$) and no significant differences were seen between 1nmol and higher doses (Figure 4B). For the 48h time-point, TBRs measured with 1nmol only differed significant from 1/16 ($p<0.05$) and 1/4nmol ($p<0.05$). Absolute signals in both tumour and background decreased significantly within the first 4 hours after injection of 1 and 5 nmol. The 5 nmol dose group showed a 4 times higher fluorescent intensity (Figure 4C).

Figure 4D shows examples of images captured with the intraoperative Artemis imaging system. Increasing the dose over 5nmol only resulted in higher fluorescent signals in both tumours and background, and not necessarily in higher TBRs (Figure S5).

Clinical relevant orthotopic models

In the orthotopic breast cancer (MCF-7) model TBRs increased significantly up-to 48h (Figure 5A) after injection of 1nmol F(ab)/800CW. Due to the relatively short blood half-

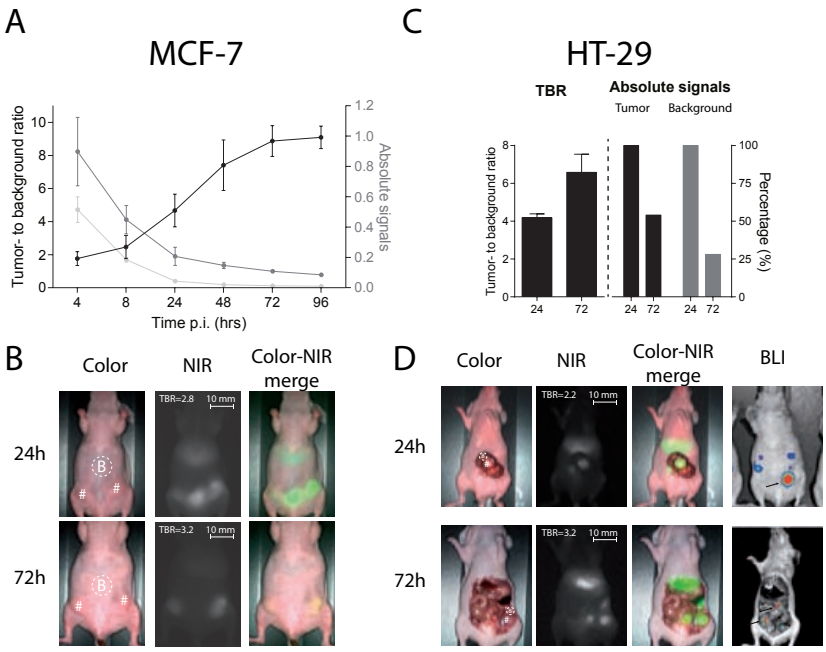

Figure 5 A) Tumour-to-background ratios and absolute signals of F(ab)/800CW in the orthotopic MCF-7 model over time. Mean TBRs were 1.76 ± 0.375, 2.46 ± 0.603, 4.67 ± 0.856, 7.41 ± 1.251, 8.87 ± 0.760 and 9.10 ± 0.558 for respectively the 4, 8, 24, 48, 72 and 96h time-point in the MCF-7 model. B) Examples of images acquired with the Artemis 24 and 72h. In white, the background regions are shown used to calculate TBRs. C) Tumour-to-background ratios at 24 and 72h and mean absolute signals at these time-points of 0.51 ± 0.084 and 0.122 ± 0.022 at 24h post injection (shown as 100%) for respectively the tumour and the background, and 0.28 ± 0.067 and 0.04 ± 0.007 at the 72h time point are shown. D) Examples of images taken with the intraoperative Artemis camera and BLI confirmed that the fluorescent lesions contained colorectal tumour cells (Organs were slightly altered between fluorescent and BLI measurements. In white, the background regions used to calculate TBRs (# tumours of different sizes).

life time (2-4 hours), the absolute signal in the background decreased faster than the signal in the tumour. Figure 5B shows an example of *in vivo* breast tumour detection using the Artemis imaging system. Tumours could be clearly recognized at 24h and 72h post injection and images from all time-points are shown in Figure S6. In the colorectal cancer model, mean TBRs increased significantly between 24h and 72h time-points (4.2±0.2 at 24h vs. 6.6±0.8 at 72h, $p<0.05$) after injection of 1nmol of F(ab)/800CW (Figure 5C). Similar as the breast cancer model, the absolute signal in the background decreased faster than the signal in the tumours between 24h and 72h (46% versus 72%). Figure 5D shows examples of images captured by the Artemis imaging system and bioluminescence, confirming the presence of tumour tissue. Moreover, micrometre-sized fluorescent nodules could be clearly visualized.

Tumour penetration

Fluorescence microscopy revealed a clear difference in fluorescence pattern and intensity between the 1, 4, 8 and 24h time-points (Figure 6). After 1 hour fluorescence was mainly present in a rim around the tumour cells. After 4 hours, fluorescence was seen throughout the whole tumour indicating full penetration of F(ab)/800CW in tumours

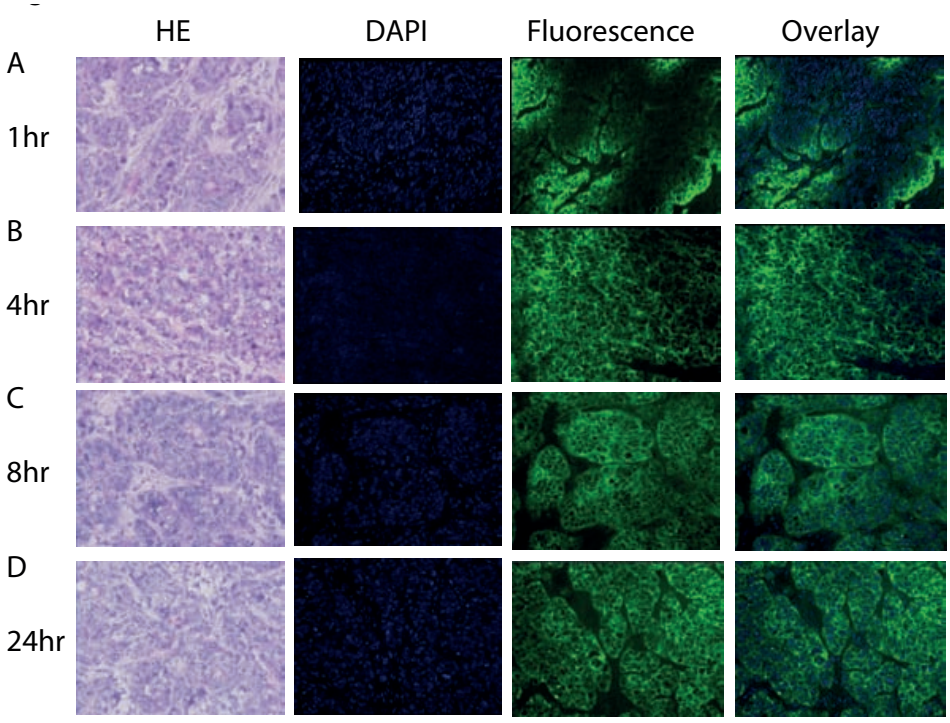

Figure 6 Fluorescence histology of HT29-tumors, obtained 1, 4, 8, and 24hours after injection of 10nmol F(ab)/800CW. Shown are respectively HE staining, DAPI staining, fluorescence microscopy images and overlay images (DAPI and fluorescence). A) Tumour penetration of F(ab)/800CW 1 hour after injection. Shown is the rim pattern type of fluorescence surrounding the tumour B) Tumour penetration of F(ab)/800CW 4 hours after injection. C) Tumour penetration of FAB/800CW 8 hours after injection D) Tumour penetration of F(ab)/800CW 24 hours after injection. Fluorescence is still clearly visible throughout the entire tumour.

between 1 and 4 hours after injection. Moreover, the level of fluorescence intensity retained in tumours between 4 and 24 hours, possibly due to internalization of the agent.

DISCUSSION

This study investigates a novel EpCAM-recognizing fluorescent agent that can demarcate breast and colorectal tumours *in vivo* using real-time fluorescence imaging. Due to the general and high overexpression on carcinomas, EpCAM is recognized as one of the most prominent pluripotent tumour targets as also recently recognized by the National Cancer Institute [14, 23]. Highest expression patterns are found in (colo)rectal cancers and their metastasis [10] and levels of over-expression are in the range of HER2/Neu ($8*10^5$-10^6 per cell), the well-established biomarker for breast cancers. Furthermore, we show that EpCAM expression is preserved after neoadjuvant therapy, a crucial characteristic for a potential candidate oncotarget. Various EpCAM specific antibodies are already clinically tested for their anti-cancer effects but little overall survival benefit was shown and affinity related side effects were observed hampering their clinical utility [24].
For almost two decades, EpCAM is evaluated as a target for imaging applications utilizing antibodies, antibody fragments and aptamers conjugated to fluorescent dyes, isotopes or both [25-28]. Zhu et al. described the use of an EpCAM-specific NIR fluorescent imaging agent for the recognition of tumour margins in a human prostate cancer orthotopic mouse model and showed accurate detection of both primary and metastatic lesions [29]. We recently conjugated the monoclonal antibody 323/A3 to IRDye800CW and showed clear tumour demarcation in breast, head-and-neck and colorectal cancer xenograft models at 72h post injection [30]. Although antibodies are believed to possess superior binding characteristics compared to smaller molecules [31, 32], their relatively large size (~150kDa) results in heterogeneous tumour distribution, liver clearance and long imaging lead-times (up-to 72h) as shown in this and our previous study [21]. F(ab) fragments are 3 times smaller and show homogenous tumour penetration. Moreover, they possess shorter half-life times and lowered immunotoxicity [33, 34] and are large enough to maintain high plasma levels for optimal (tumour) distribution [35-37].
The novel described EpCAM-specific imaging agent is designed for clinical use. Experiments were therefore performed with a clinically validated imaging system, vehicle and NIR fluorescent dye to expedite effective clinical translation. The antibody fragment we specifically developed, is a deimmunized F(ab) fragment of its full antibody variant 4D5 MOC-B to address immunogenicity [38]. A non-deimmunized variant, fused with a deimmunized variant of the plant-derived toxin bouganin, was already used in a first-in-human clinical trial recently [18]. Conjugation was performed by the well-established/accepted NHS-method, using conditions leading to stable dye/protein-labelling ratios

of around 1.5. Affinity assays on human recombinant EpCAM and EpCAM positive cells indicated that labelling ratios lower than 1 or higher than 2 were less efficient. (Pre) Clinical studies showed that IRDye800CW is not immunogenic with a no adverse effect level (NOAEL) of 20mg/kg [39, 40]. The advantage of IRDye800CW with respect to other NIR-fluorescent dyes is the good water-solubility in combination with high signal intensity. Water-solubility enables conjugation in water-based solutions, which simplifies the purification process substantially. This is important for production under GMP conditions and enhances clinical translation. The conjugate was found to be stable at 2 mg/ml in PBS, stored at -20°C. Various test conditions, including storage at RT/37°C for 24 hours, lyophilisation and multiple freeze/thaw procedures did not affect the stability or affinity. The limited effect of the enhanced permeability and retention (EPR) effect was shown using *in vivo* blocking experiments, where a 3-4 times lower TBR was measured after pre-injection of unlabelled agent. The stagnating TBRs in the higher dose groups (5-20nmol) clearly showed the concentrations at which all available EpCAM molecules of the tumour were occupied. Since we used a cell-line with very high EpCAM expression (HT-29), it can be rationalized that the 1-5 nmol doses will be sufficient for clinical use. Moreover, a dose of 1-5 nmol in mice (50-250µg) corresponds with a dose of 0.16-0.8 mg/kg in humans, as converted using the body-surface area method [41].

Biodistribution showed a classical F(ab) distribution pattern with high TBRs and high signals in the tumour and excreting organs. Due to the glomerular-filtration cut-off of 60 kDa, most of the agent is excreted via the kidneys. The observed high fluorescent signals in the liver may be explained by the lipophilicity and negative charge of IRDye800CW, which leads to increased albumin binding and adjacent liver accumulation. Moreover, no significant liver uptake could be measured with indium [42]. The half-life time of F(ab)/800CW was estimated at 2-4 hours, which is in concordance with VB6-845 in humans [18]. Although the total circulation time of F(ab)/800CW will be short (10-20h), it is sufficient to allow adequate tumour penetration as after 1-4h homogenous intracellular signals throughout the tumour was already seen. Although internalization is not strictly needed, it is advantageous for the purpose of imaging, because it extends the imaging window. Using the Artemis intraoperative camera system, two clinically relevant orthotopic mouse models were investigated. Real-time tumour-specific visualization of (colo) rectal and breast tumours was shown with high TBRs between 8-24 hours.

Before clinical introduction of this novel agent can be realized, a generic single extended dose toxicology study must be performed. This will be considered to be sufficient as no cross-reactivity is expected due to species-specific EpCAM expression. After first-in-human (Phase 0) and feasibility dose-escalation (Phase 1) trials, a Phase 2 trial can be designed that randomizes patients between surgery with and without the EpCAM-targeted imaging agent. Outcomes must contain survival, R0 vs R1 resection and coherence with pathological findings. Suitable patients can be straightforward preoperatively

selected with immunohistochemistry on biopsy species using either MOC31 or the F(ab) fragment.

In conclusion, clinical application of this novel tumour-specific (NIR) fluorescent imaging agent F(ab)/800CW is expected to improve intraoperative visualization of (residual) cancer, positive lymph nodes, local metastasis and irradical resections. Wide implementation of tumour-specific (NIR) fluorescence imaging has the potential to make surgery safer and more precise. The choice for EpCAM and the appropriateness of molecular design allow rapid clinical development.

REFERENCES

1. Vahrmeijer AL, Hutteman M, van der Vorst JR, van de Velde CJ, Frangioni JV. Image-guided cancer surgery using near-infrared fluorescence. Nat Rev Clin Oncol 2013;10: 507-18.
2. van Dam GM, Themelis G, Crane LM, et al. Intraoperative tumour-specific fluorescence imaging in ovarian cancer by folate receptor-alpha targeting: first in-human results. Nat Med 2011;17:1315-9.
3. van Oosten M Crane LM, Bart J, van Leeuwen FW, van Dam GM. Selecting Potential Targetable Biomarkers for Imaging Purposes in Colorectal Cancer Using TArget Selection Criteria (TASC): A Novel Target Identification Tool. Transl Oncol 2011;4:71-82.
4. Herlyn M, Steplewski Z, Herlyn D, Koprowski H. Colorectal carcinoma-specific antigen: detection by means of monoclonal antibodies. Proc Natl Acad Sci U S A 1979;76: 1438-42.
5. Patriarca C, Macchi RM, Marschner AK, Mellstedt H. Epithelial cell adhesion molecule expression (CD326) in cancer: a short review. Cancer Treat Rev 2012;38:68-75.
6. Balzar M, Winter MJ, de Boer CJ, Litvinov SV. The biology of the 17-1A antigen (Ep-CAM). J Mol Med (Berl) 1999;77:699-712.
7. Winter MJ, Nagtegaal ID, van Krieken JH, Litvinov SV. The epithelial cell adhesion molecule (Ep-CAM) as a morphoregulatory molecule is a tool in surgical pathology. Am J Pathol 2003;163:2139-48.
8. Trzpis M, McLaughlin PM, de Leij LM, Harmsen MC. Epithelial cell adhesion molecule: more than a carcinoma marker and adhesion molecule. Am J Pathol 2007; 171:386-95.
9. Went PT, Lugli A, Meier S, et al. Frequent EpCam protein expression in human carcinomas. Hum Pathol 2004;35:122-8.
10. Spizzo G, Fong D, Wurm M, et al. EpCAM expression in primary tumour tissues and metastases: an immunohistochemical analysis. J Clin Pathol 2011;64:415-20.
11. Went P, Vasei M, Bubendorf L, et al. Frequent high-level expression of the immunotherapeutic target Ep-CAM in colon, stomach, prostate and lung cancers. Br J Cancer 2006; 94:128-35.
12. Riethmuller G, Schneider-Gadicke E, Schlimok G, et al. Randomised trial of monoclonal antibody for adjuvant therapy of resected Dukes' C colorectal carcinoma. German Cancer Aid 17-1A Study Group. Lancet 1994;343:1177-83.
13. Seimetz D, Lindhofer H, Bokemeyer C. Development and approval of the trifunctional antibody catumaxomab (anti-EpCAM x anti-CD3) as a targeted cancer immunotherapy. Cancer Treat Rev 2010;36:458-67.
14. Gires O, Bauerle PA. EpCAM as a target in cancer therapy. J Clin Oncol 2010;28: e239-e240.
15. MacDonald GC, Rasamoelisolo M, Entwistle J, et al. A phase I clinical study of VB4-845: weekly intratumoural administration of an anti-EpCAM recombinant fusion protein in patients with squamous cell carcinoma of the head and neck. Drug Des Devel Ther 2009;2:105-14.
16. Marshall MV, Draney D, Sevick-Muraca EM, Olive DM. Single-dose intravenous toxicity study of IRDye 800CW in Sprague-Dawley rats. Mol Imaging Biol 2010;12:583-94.
17. Zinn KR, Korb M, Samuel S, et al. IND-directed safety and biodistribution study of intravenously injected cetuximab-IRDye800 in cynomolgus macaques. Mol Imaging Biol 2015;17:49-57.
18. Entwistle J., Kowalski M., Brown J., MacDonald G.C. The preclinical and clinical evaluation of VB6-845: an immunotoxin with a de-immunized payload for the systemic treatment of solid tumours. Antibody-drug conjugates and immunotoxins: from pre-clinical development to therapeutic applications. Cancer Drug Discovery and Development. G.L. Phillips; 2013.
19. de Boer E Warram JM, Tucker MD, et al. *In vivo* Fluorescence Immunohistochemistry:

Localization of Fluorescently Labeled Cetuximab in Squamous Cell Carcinomas. Sci Rep 2015;5:10169.
20. Boonstra MC, Tolner B, Schaafsma BE, et al. Pre-clinical evaluation of a novel CEA-targeting near-infrared fluorescent tracer delineating colorectal and pancreatic tumours. Int J Cancer 2015.
21. Boonstra MC, Van Driel PB, van Willigen DM, et al. uPAR-targeted multimodal tracer for pre- and intraoperative imaging in cancer surgery. Oncotarget 2015.
22. Van Driel PB, van de Giessen M, Boonstra MC, et al. Characterization and evaluation of the artemis camera for fluorescence-guided cancer surgery. Mol Imaging Biol 2015;17: 413-23.
23. Cheever MA, Allison JP, Ferris AS, et al. The prioritization of cancer antigens: a national cancer institute pilot project for the acceleration of translational research. Clin Cancer Res 2009;15:5323-37.
24. Munz M, Murr A, Kvesic M, et al. Side-by-side analysis of five clinically tested anti-EpCAM monoclonal antibodies. Cancer Cell Int 2010; 10:44.
25. Hall MA, Kwon S, Robinson H, Lachance PA, Azhdarinia A, Ranganathan R, et al. Imaging prostate cancer lymph node metastases with a multimodality contrast agent. Prostate 2012 Feb 1;72(2):129-46.
26. Hall MA, Pinkston KL, Wilganowski N, Robinson H, Ghosh P, Azhdarinia A, et al. Comparison of mAbs targeting epithelial cell adhesion molecule for the detection of prostate cancer lymph node metastases with multimodal contrast agents: quantitative small-animal PET/CT and NIRF. J Nucl Med 2012 Sep;53(9):1427-37.
27. Shigdar S, Lin J, Yu Y, Pastuovic M, Wei M, Duan W. RNA aptamer against a cancer stem cell marker epithelial cell adhesion molecule. Cancer Sci 2011 May;102(5):991-8.
28. Tavri S, Jha P, Meier R, Henning TD, Muller T, Hostetter D, et al. Optical imaging of cellular immunotherapy against prostate cancer. Mol Imaging 2009 Jan;8(1):15-26.
29. Zhu B, Wu G, Robinson H, Wilganowski N, Hall MA, Ghosh SC, et al. Tumor margin detection using quantitative NIRF molecular imaging targeting EpCAM validated by far red gene reporter iRFP. Mol Imaging Biol 2013 Oct;15(5):560-8.
30. van Driel PB, Boonstra MC, Prevoo HA, van de Giessen M, Snoeks TJ, Tummers QR, et al. EpCAM as multi-tumour target for near-infrared fluorescence guided surgery. BMC Cancer 2016 Nov 14;16(1):884.
31. Wittrup KD, Thurber GM, Schmidt MM, Rhoden JJ. Practical theoretic guidance for the design of tumour-targeting agents. Methods Enzymol 2012;503:255-68. 26. Freise AC, Wu AM. *In vivo* imaging with antibodies and engineered fragments. Mol Immunol 2015.
32. Gratz S, Reize P, Kemke B, Kampen WU, Lusteri M, Hoffken H. Targeting of osteomyelitis with IgG and Fab' Monoclonal Antibodies Labeled with [99mTc]: kinetic evaluations. Q J Nucl Med Mol Imaging 2014.
33. Kosaka N, Ogawa M, Paik DS, Paik CH, Choyke PL, Kobayashi H. Semiquantitative assessment of the microdistribution of fluorescence-labeled monoclonal antibody in small peritoneal disseminations of ovarian cancer. Cancer Sci 2010;101:820-5.
34. Pak KY, Nedelman MA, Fogler WE, et al. Evaluation of the 323/A3 monoclonal antibody and the use of technetium-99m-labeled 323/A3 Fab' for the detection of pan adenocarcinoma. Int J Rad Appl Instrum B 1991;18:483-97.
35. Watanabe R, Hanaoka H, Sato K, et al. Photoimmunotherapy targeting prostate-specific membrane antigen: are antibody fragments as effective as antibodies? J Nucl Med 2015;56:140-4.
36. Mendler CT, Friedrich L, Laitinen I, et al. High contrast tumour imaging with radio-labeled antibody Fab fragments tailored for

optimized pharmacokinetics via PASylation. MAbs 2015;7:96-109.
37. Li D, Liu S, Liu R, et al. EphB4-targeted imaging with antibody h131, h131-F(ab')2 and h131-Fab. Mol Pharm 2013;10:4527-33.
38. Willuda J, Honegger A, Waibel R, et al. High thermal stability is essential for tumour targeting of antibody fragments: engineering of a humanized anti-epithelial glycoprotein-2 (epithelial cell adhesion molecule) single-chain Fv fragment. Cancer Res 1999;59:5758-67.
39. Marshall MV, Draney D, Sevick-Muraca EM, Olive DM. Single-dose intravenous toxicity study of IRDye 800CW in Sprague-Dawley rats. Mol Imaging Biol 2010;12:583-94.
40. de Boer E, Warram JM, Tucker MD, et al. *In vivo* Fluorescence Immunohistochemistry: Localization of Fluorescently Labeled Cetuximab in Squamous Cell Carcinomas. Sci Rep 2015;5:10169.
41. Reagan-Shaw S, Nihal M, Ahmad N. Dose translation from animal to human studies revisited. FASEB J 2008;22:659-61.
42. Valko K, Nunhuck S, Bevan C, Abraham MH, Reynolds DP. Fast gradient HPLC method to determine compounds binding to human serum albumin. Relationships with octanol/water and immobilized artificial membrane lipophilicity. J Pharm Sci 2003;92:2236-48.